Hydraulic fracture width determination using integration of Stoneley wave "pressure testing" with electrical borehole scans in FORGE Geothermal project

Brian E. Hornby, Hornby Geophysical Services, LLC*

Summary

In a well drilled in the DOE FORGE Geothermal test site both electrical borehole scans acquired using Schlumberger's Formation Micro-scanner Image tool (FMI) and Stoneley waves generated by a borehole sonic tool are used together in a workflow using the strengths of both techniques to characterize fractures crossing the well and estimate their effective width. In this work separate fracture width estimations for both FMI and Stoneley wave analyses are compared, and conclusions drawn on the relative merits. Next, a workflow was created to use the FMI determined fracture locations to drive the Stoneley wave analysis and results were presented for different sections with FMI images for reference. Finally, an improved workflow was established to deliver a robust estimation of hydraulic fracture width using all the available data.

Introduction

Clean energy production using Enhanced Geothermal Systems (EGS) is an area that has had a lot of recent attention. The theory is simple – shown in Figure 1 is a picture detailing the process, extracted from a U.S. Department of Energy (DOE) overview on the subject. Here a man-made reservoir is created where there is hot rock and little or no natural permeability. Well stimulation is used to cause pre-existing fractures to open and so allow transport of water through the rock to the production wells which pass the heated water to the surface where electricity is generated.

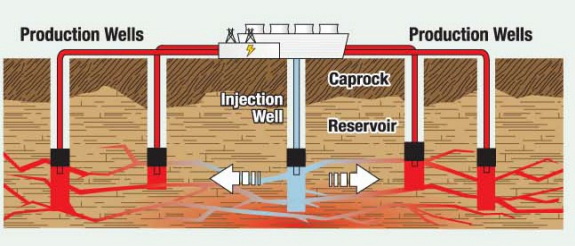

To spur development of innovative technologies the Utah Frontier Observatory for Research in Geothermal Energy (FORGE) was created (Moore et al., 2018). In 2017 well 58-32 was drilled and extensively logged. Electrical borehole scans were obtained using Schlumberger's Formation Micro-scanner Image tool (FMI). Analysis of these data were crucial to identify local stress directions and locate natural and drilling-induced fractures crossing the borehole. The formations are extensively fractured, with more than 2000 natural and 356 induced fractures identified. In addition, FMI data recorded in the lower 130 ft section of the well were analyzed for hydraulic fracture width across the scanned fracture openings using a method based on quantification of the additional current flow injected into the fracture (Luthi and Souhaité, 1990). A limitation of FMI fracture width determination is that measurements are at the borehole wall and analysis cannot differentiate between fractures connected beyond the borehole and fractures terminating near the borehole. To complement the FMI fracture width result Stoneley wave data is used for deeper investigation of conductive fractures using secondary arrivals caused by pressure release into the fractures (Hornby et al., 1989). In essence the Stoneley wave is used to "pressure test" the fractures as identified by the FMI analysis and processing also provides an estimate of hydraulic fracture width. An objective of this work is to create an integrated workflow using both measurements to create high-quality estimations of hydraulic fracture widths of conductive fractures crossing a borehole. These results can then be used to high-grade borehole sections for well stimulation, for example.

Method

To probe fractures with Stoneley wave signals it is imperative to generate the waves at low frequencies, ideally below 500 Hz. With low frequencies the Stoneley reflectivity will mostly respond to conductive fractures and essentially will ignore fracture opening enhancements or small borehole enlargements (Kostek et al., 1998a; Kostek et al., 1998b). Large borehole size changes or washouts will affect the Stoneley wave response and so quality control using borehole caliper or hole volume measurements are needed. In addition high-frequency (say 2000 to 3000 Hz ranges) Stoneley wave processing can deliver useful curves that can be used to highlight intervals of possible issues. Here sudden increases in the high frequency reflectivity with hole size changes gives a clear indications results are suspect for that interval.

Sonic data were acquired using Schlumberger's DSST tool. To acquire Stoneley waves a low frequency monopole source drive was used which fires into 8 receivers at ½ ft spacing between each receiver and with a 9 ft spacing from the monopole source to the first receiver. Figure 2 shows a plot of acquired waveforms at a single depth and Figure 3 shows a spectral analysis result for receiver 1. Good news is

that peak energy is a 500 Hz and usable data (-20 dB) is from about 300 to 3000+ Hz which supports use of these data to estimate fracture widths.

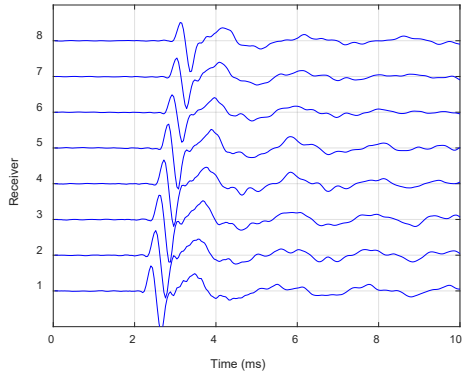

Figure 2. Full-waveform data acquired across the array

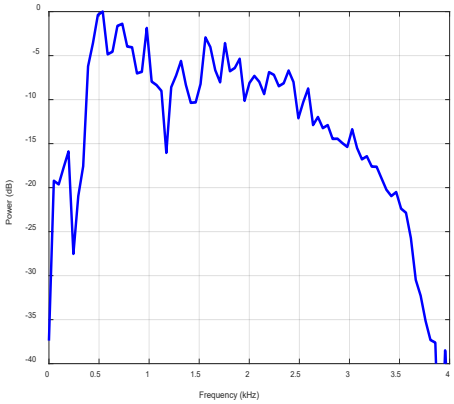

Figure 3. Spectral analysis of Stoneley wave data.

In Figure 4 are iso-offset plots for a single source receiver pair as a function of depth along with reference gamma-ray and caliper curves. Column 3 shows the recorded data, where clear signals from conductive fractures are seen with the oblique arrivals (Chevron events). Processing flow involves filtering to separate the direct arrivals and then a deconvolution process computes the Stoneley reflectivity response from the fracture. The magnitude of this signal is then used to create a reflectivity curve for every frequency range processed. Here the core processing is the lowest frequency signal you can achieve, here centered at 500 Hz. For quality control and to understand any borehole effects processing is also done at higher frequency bands (Hornby et al. 1999); in this case frequencies of 2000 Hz and 3000 Hz were processed.

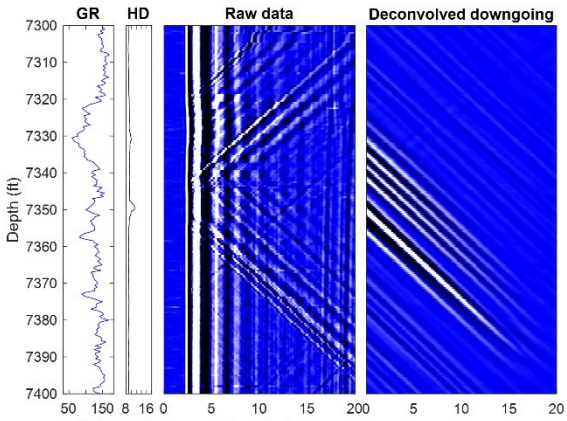

Figure 4. Reference gamma-ray and caliper logs along with single receiver iso-offset sections of recorded Stoneley wave data and final processed down-going Stoneley reflectivity response.

Results and interpretation

Comparison of FMI and Stoneley wave fracture width results over the bottom hole section are shown in Figure 5. FMI fracture width is processed for interpreted conductive or partially conductive fracture locations and overlaid directly on the continuous curve of the Stoneley wave fracture width estimation. Peaks in this curve are often consistent with borehole image log interpreted fracture locations. On the right side are FMI images for different intervals, with the image depth range on the log depth axis indicated by the solid bars. Comparison of the two results shows an excellent match over much of the interval, consistent with an earlier case study (Hornby et al., 1992). Looking now at individual sections, we see that from the bottom of the well up to the fracture at 7498 ft (red colored overlay on FMI image) the FMI fracture width result overlays the Stoneley wave result. Above that level up to 7460 ft there are some good comparisons however many FMI fracture widths are higher, with some levels appearing anonymously high. These results are not supported by the Stoneley wave results and possibly indicate events with enhanced openings or other effects such as tool excentering. Next the section from 7460 to 7440 ft the two methods overlay quite nicely – giving us a high confidence in the result. The next interval has the large Stoneley wave event peaking at 7439 ft. The FMI image for that section does not show support for open fractures there, and so here the Stoneley is likely affected by borehole size changes giving an anomalous result. This is supported by the caliper log which shows a step change at the level and also supported

by the high frequency Stoneley reflectivity curves showing an increase, indicating likely effects from borehole size changes. In the final section up to the top depth we see again a reasonable agreement between the two results with one interesting exception. The drilling induced fractures are mostly seen with larger FMI interpreted fracture widths than seen with the Stoneley wave result. This is consistent with normal expectations due to the nature of the event. Here the integrated interpretation is that the FMI interpreted width at the borehole wall is not supported to be connected deeper into the formation by the Stoneley wave result. There can be exceptions to this – especially if the drilling induced fracture connects near the wellbore to natural fracture networks.

The next example shown in Figure 6 does not have any FMI derived fracture width estimates. And so here results are integrated in a different manner – for each fracture interpreted by the FMI analysis fracture width is taken from the Stoneley result. Here two types of fractures are taken from the FMI analysis. FMI interpreted conductive or partially conductive fractures are grouped together and plotted with a blue "x" symbol and interpreted drilling induced fractures are red circles. Here the conductive fracture locations show varying fracture widths up to 2 mm. This is supported by the bottom image which clearly shows a large number of well-defined natural fractures. Moving up we see a sequence of drilling induced fractures which show little or no effective fracture width, again consistent with expectations for unconnected drilling-induced fractures. Finally at the top of the interval we see a strong response on the Stoneley wave reflectivity and fracture width peaking at 7223 ft. FMI interpretation shows a single conductive fracture event at the same depth with the Stoneley result show a fracture width of 1.5 mm. Looking at the FMI image we see what looks like a higher angle fracture just below that fracture and so there may be another event or two contributing to the Stoneley response.

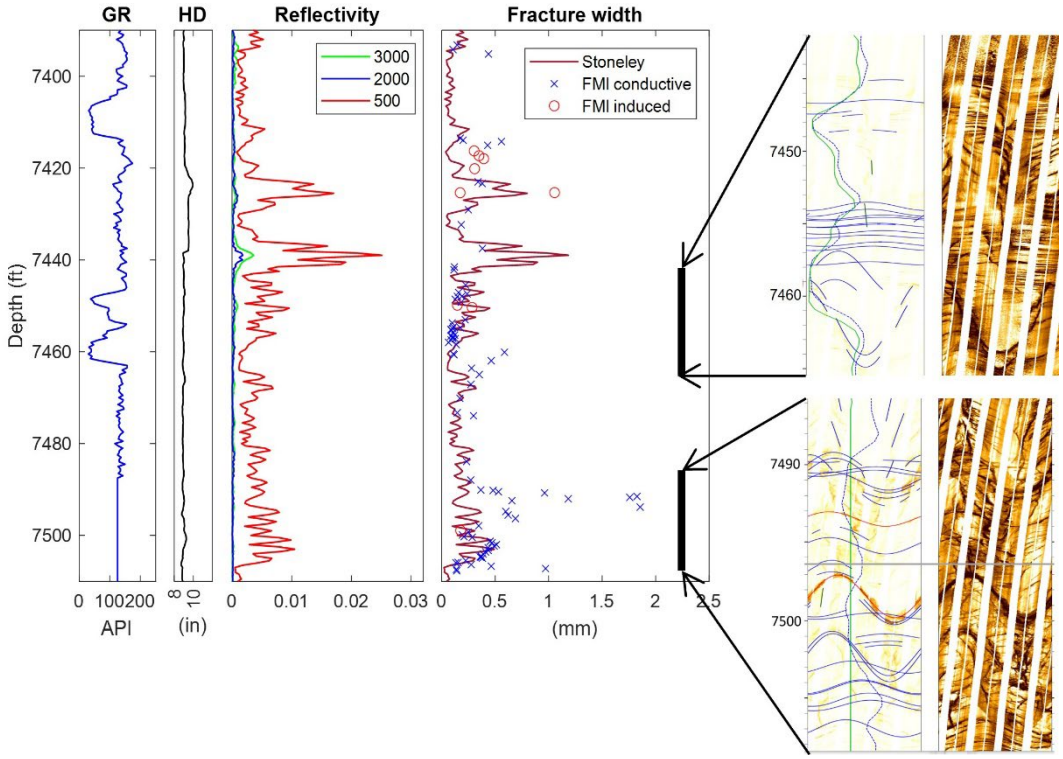

Figure 5. Comparison of FMI and Stoneley wave fracture width results with reference gamma-ray and caliper logs over the bottom hole section. Column 3 shows Stoneley reflectivity response for three frequencies and column 4 is an overlay of FMI estimated fracture widths at interpreted fracture locations with a depth continuous Stoneley wave fracture width estimation. Reference pictures of FMI borehole scans are on the right.

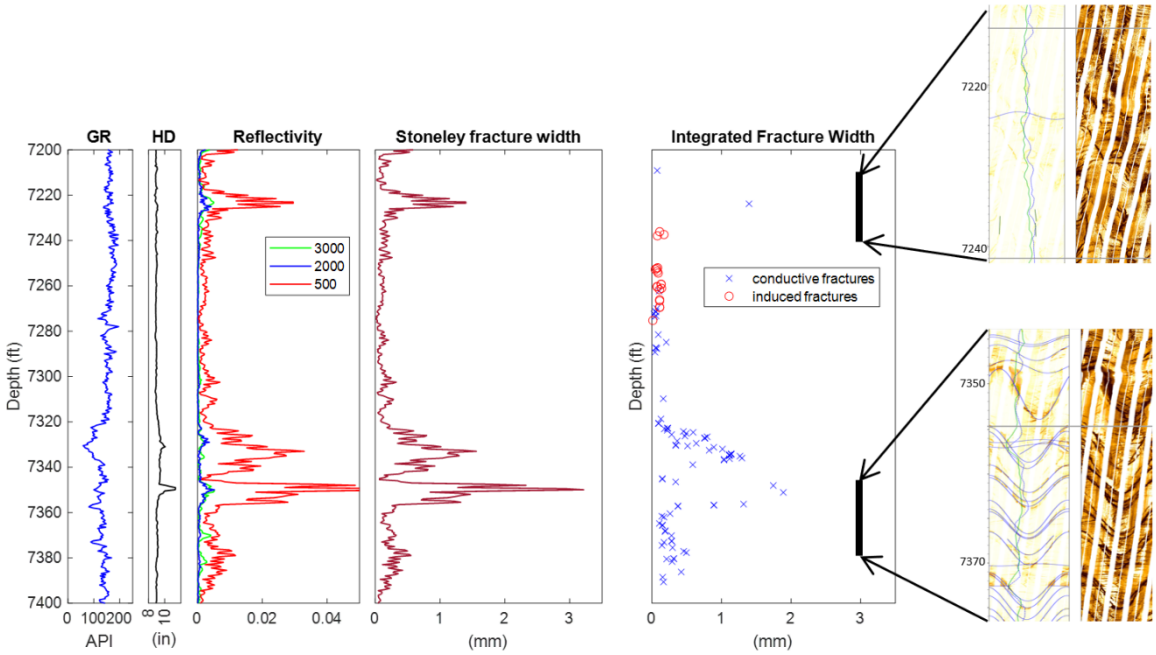

Figure 6. Comparison of FMI and Stoneley wave fracture width results with reference gamma-ray and caliper logs over the bottom hole section. Column 3 shows Stoneley reflectivity response for three frequencies and column 4 is a plot of depth continuous Stoneley derived fracture width. Column 5 shows FMI interpreted conductive or induced fractures with effective fracture width taken from the Stoneley wave result.

Finally – this work leads to an improved workflow for robust estimation of hydraulic fracture widths.

1. All fracture width results need to be driven by quality analysis of borehole image logs, preferable electrical borehole scans, showing conductive or partially conductive fractures crossing the well, either natural or induced.
2. Where FMI and Stoneley fracture widths are similar, results can be taken from either tool with high confidence or an average used.
3. If either result looks anomalous – for example large FMI fracture widths with no real support from the image display or large Stoneley wave response where there is no support from the image display or a large borehole washout is interpreted, then drop the anomalous result.
4. If the Stoneley result is lower than the FMI estimation, then use the Stoneley result. This indicates that the fracture is truncated near the borehole which is most often seen with drilling induced fractures but can occur with natural fractures.
5. If a good quality Stoneley determined fracture width is higher this could mean the fracture is connected beyond the borehole wall, supporting a higher effective fracture width.
6. If FMI fracture width analysis is not available, FMI locations of conducting and induced fractures are populated with the Stoneley wave results.

Conclusions

Data collected in well 58-32 in DOE's FORGE Geothermal test site were processed for Stoneley wave reflectivity and fracture width, assuming a parallel plate model. Results were compared with fracture widths estimated from FMI images across interpreted conductive fracture locations. This comparison was informative – showing in large sections an encouraging overlay of both estimated fracture widths. In other places there were differences. With drilling induced fractures the Stoneley wave result was lower indicating the induced fractures truncated close to the borehole wall as expected. Other differences were attributed to anomalous results by either technique. In sections where FMI fracture widths were not computed, FMI fracture locations were simply populated with Stoneley wave results. These learnings lead to an improved workflow for robust fracture width estimation.

Acknowledgements

Open-source data were provided by U.S. DOE Geothermal Data Repository. I thank Greg Nash, University of Utah, for his help obtaining complete data files for this project.

References

Hornby, B. E., D. L. Johnson, K. W. Winkler, and R. A. Plumb, 1989, Fracture evaluation using reflected Stoneley wave arrivals: Geophysics, **54**, no. 10, 1274–1288, doi: https://doi.org/10.1190/1.1442587.

Hornby, B. E., S. M. Luthi, and R. A. Plumb, 1992, Comparison of fracture apertures computed from electrical borehole scans and reflected Stoneley waves: An integrated interpretation: The Log Analyst, **33**, no. 1.

Hornby, B. E., J. A. Lorsong, R. Wydrinski, and A. Vittachi, 1999, Integrated fracture analysis using borehole geophysical techniques: SPWLA 40th Annual Meeting.

Kostek, S., D. L. Johnson, and C. J. Randall, 1998, The interaction of tube waves with borehole fractures, Part I: Numerical models: Geophysics, **63**, no. 3, 800–808, doi: https://doi.org/10.1190/1.1444391.

Kostek, S., D. L. Johnson, K. W. Winkler, and B. E. Hornby, 1998, The interaction of tube waves with borehole fractures, Part II: Analytical models: Geophysics, **63**, no. 3, 809–815, doi: https://doi.org/10.1190/1.1444392.

Luthi, S. M. and P. Souhaité, 1990, Fracture apertures from electrical borehole scans, Geophysics, **55**: 821833, doi: https://doi.org/10.1190/1.1442896.

Moore, J., J. McLennan, K. Pankow, S. Simmons, R. Podgorney, P. Wannamaker, C. Jones, W. Rickard, and P. Xing, 2019, The Utah Frontier Observatory for Research in Geothermal Energy (FORGE): A laboratory for characterizing, creating and sustaining enhanced geothermal systems: Proceedings, 45th Workshop on Geothermal Reservoir Engineering, SGP-TR-216.